J. Fluid Mech. (2001), *vol.* 436, *pp.* 249–266. Printed in the United Kingdom

© 2001 Cambridge University Press

Hydrodynamics of locomotion in the squid *Loligo pealei*

By ERIK J. ANDERSON[1]†, WILLIE QUINN[2] AND M. EDWIN DeMONT[1]‡

[1]Biology Department, St. Francis Xavier University, PO Box 5000, Antigonish, Nova Scotia, Canada B2G 2W5

[2]Engineering Department, St. Francis Xavier University, PO Box 5000, Antigonish, Nova Scotia, Canada B2G 2W5

(Received 15 July 1999 and in revised form 20 December 2000)

Potential flow analysis, including unsteady effects, has been applied to live swimming squid, *Loligo pealei*. Squid were modelled as slender, axisymmetric bodies. High-speed video records, recorded at frame rates of 125 to 250 Hz, provided time-varying body outlines which were digitized automatically. Axisymmetric renderings of these body outlines and the real motion of the squid were used as the input of the potential flow analysis. Axial and lateral inviscid fluid forces simply due to the flow past the squid body were calculated from pressures coefficients obtained from the unsteady Bernoulli equation. Lateral forces were found to play virtually no role in determining muscle stresses in squid jet propulsion. Axial pressure forces were also found to be small in comparison to both net force (based on the observed whole body kinematics) and estimations of skin friction. These findings demonstrate the effects of the highly adapted shape of squid with regard to hydrodynamics. The work suggests that skin friction and working fluid intake are the most significant sources of drag on a swimming squid.

1. Introduction

Squid swim using jet propulsion and undulating fins. The jet is powered by circumferentially arranged muscles in the walls of the squid mantle. Water in the mantle cavity is pressurized by the contraction of these muscles and expelled as a jet (figure 1). The squid is propelled through the water with its mantle leading and arms trailing. In sustained swimming, mantle-first swimming is the norm, but a squid can point its jet in various directions and propel itself arms-leading, as well. After jetting, the squid refills its mantle cavity with seawater to prepare for the next jet event. The method of mantle refill is believed to be the result of elastic properties of the mantle tissue (Gosline & Shadwick 1983), the action of antagonistic muscles called radial muscles (Gosline *et al.* 1983), and flow-induced surface pressures (Vogel 1987). The intake and jetting of water is regulated by a structure known as the funnel, which acts as a one-way valve. *L. pealei* has two triangular-shaped fins at the apex of the mantle (figure 2). Waves generally travel along the fins in the direction opposite to the velocity of the squid through the water in order to produce thrust (Hoar *et al.*

† Present address: Department of Applied Ocean Physics and Engineering, Woods Hole Oceanographic Institution, Woods Hole, MA 02543, USA.

‡ Author to whom correspondence should be addressed, e-mail: edemont@stfx.ca

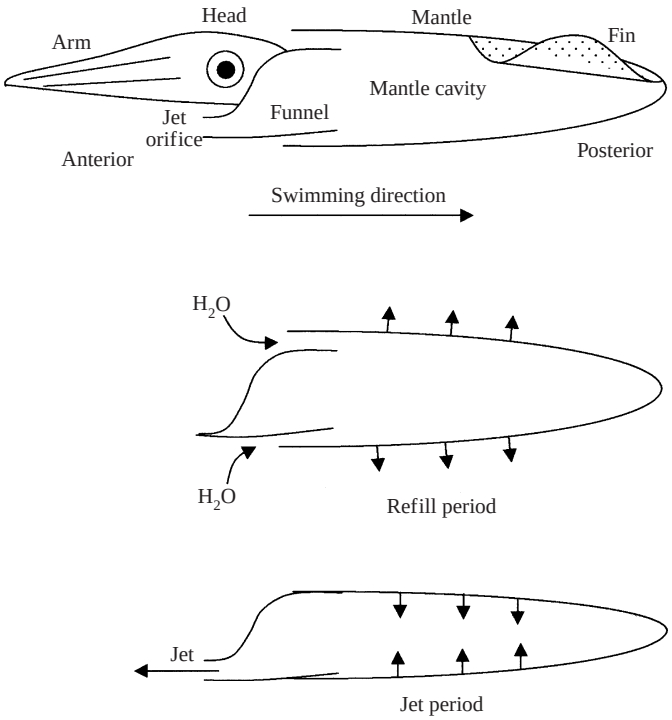

FIGURE 1. Structure and mechanics of squid propulsion. Small arrows indicate the motion of the mantle wall during the jet and refill periods. The jet orifice is closed during refill.

1994). This was recently confirmed by Anderson (1998) from highly resolved fin wave velocity compared to whole body velocity and acceleration.

Squid also display a behaviour known as escape jetting, which is used to escape predators and other dangers (Williamson 1965). In this behaviour, the squid hyperinflates and then contracts its mantle powerfully (Gosline & DeMont 1985). This process is commonly repeated a few times when the squid is attempting to escape danger. During escape jetting squid keep their fins wrapped tightly against themselves (Williamson 1965). In this investigation, however, the focus is on sustained swimming, as would be observed in migrations (Shevtsov 1973).

It was not until about 1960 that investigators began to take a serious look at the kinematics and dynamics of squid locomotion. It was then that Siekman (1962) derived hydrodynamic equations for pulsating jets, and Zuev (1963, 1964, 1965, 1966*a*) examined the roles of body shape, locomotory mode, hydrodynamic forces, and buoyancy in squid swimming. Zuev (1966*b*) united these parameters in a classical dynamic analysis of squid swimming and manoeuvring inspired by the fish hydrodynamics work of Aleev (1962). Several years of intense experimental and theoretical study ensued concerning squid jet propulsion, mantle muscle action, nervous control mechanisms, connective fibre behaviour, intramantle pressure, thrust, gait, mantle deformation, maximum attainable speeds, and accelerations (Wilson 1960; Williamson 1965; Johnson & Soden 1966; Bradbury & Aldrich 1969; Johnson, Soden & Trueman 1972; Ward & Wainwright 1972; Ward 1972; Shevtsov 1973; Packard & Trueman 1974; Weihs 1977).

In the area of kinematics, there exists a humorous folklore of proposed swimming velocities based on a range of observations from rough estimates made by divers

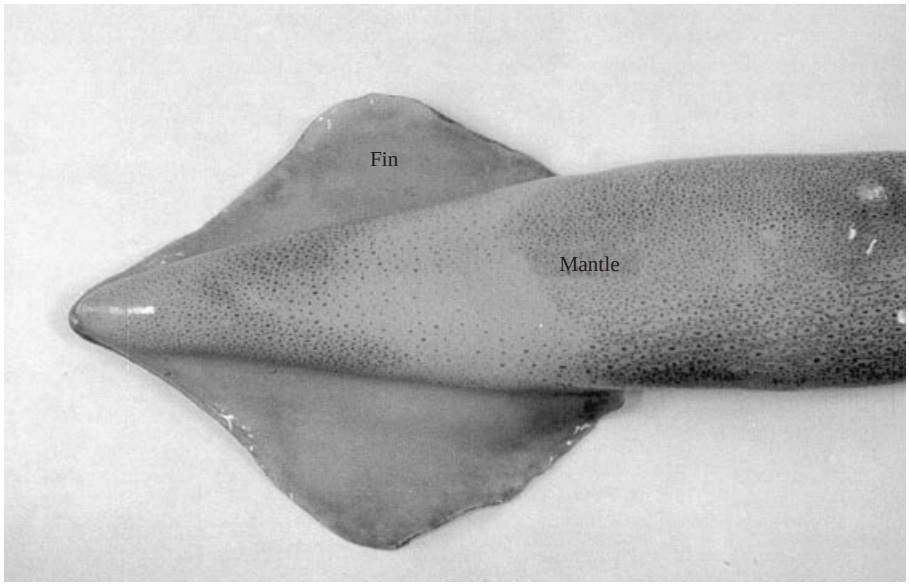

FIGURE 2. A view of the fins of squid looking at the ventral surface of the mantle. The fins are attached along the dorsal surface of the mantle.

(Williamson 1965) to projectile motion calculations on squid observed clearing ship rails (Lane 1957). Cole & Gilbert (1970) recorded squid swimming and leaping squid at frame rates of 16 to 30 per second (FPS). Packard (1969) used stroboscopic techniques to photograph squid swimming using strobe frequencies of 50 Hz. Most of the existing swimming records, however, are of limited use due to one of two experimental conditions – the use of still-water tanks or relatively small-diameter swimming tunnels. Investigators using still-water tanks complain of difficulties in keeping squid in the fields of view of their cameras (Packard 1969), and in narrow swim tunnels squid are reported to come into contact with walls and restraining grates occasionally (O'Dor 1982). The combination of these limitations together with resolution limits due to frame rates and shutter speeds, has interfered with the gathering of swimming records from which simultaneous, whole-cycle, kinematic and body deformation data can be accurately extracted.

Several investigators have measured kinematic and body deformation data in squid locomotion separately (Trueman & Packard 1968; Packard 1969; Ward 1972; Gosline *et al.* 1983). In general, body kinematics were measured from records of free-swimming animals, while mantle deformation was measured from records taken while the animals were physically restrained. Aside from the problems inherent in the assumption that deformations in restrained squid are the same as those in swimming squid, these investigators lacked digital image analysis equipment capable of efficiently extracting the entire deforming outline of the squid. Thus, methods of acquiring body deformation data in earlier studies were confined to tracing squid profiles by hand (Ward 1972), and measuring mantle diameters at single positions with a video dimension analyser (Gosline *et al.* 1983).

The study of squid hydrodynamics has been virtually non-existent since 1977. The primary exceptions are Vogel (1987), O'Dor (1988) and Hoar *et al.* (1994). Vogel (1987) experimentally measured steady mantle surface pressures over an axisymmetric squid-shaped model. O'Dor (1988) applied kinematic and dynamic data from swim

tunnel work to the earlier squid propulsion models of Zuev (1966*b*), Johnson *et al.* (1972) and Weihs (1973, 1977). Hoar *et al.* (1994) looked at fin-based locomotion in squid. Nevertheless, Vogel (1987) and O'Dor (1988) admit, as did Zuev (1966*a*), that the hydrodynamics of squid locomotion are inherently unsteady, and thus demand further investigations that account for unsteady effects. The application of unsteady hydrodynamics to aquatic locomotion was treated in detail by Daniel (1984). He reinforced the fact that swimming in animals is predominantly unsteady. In his survey of unsteady fluid forces, Daniel (1984) concentrated on added mass, or the acceleration reaction. Lighthill (1960) included the effects of added mass in his analysis of fish swimming. Daniel (1984) devotes a section of his review of the acceleration reaction to squid and other jet-propelled organisms and claims that, although for periodically jetting organisms the average added mass effect is zero, unsteady analyses are essential to determining instantaneous fluid forces acting in such systems.

The recent work of Cheng, Davison & DeMont (1996), and Cheng & DeMont (1996*a*, *b*) on the jet-propelled swimming scallop is an example of this sort of complete unsteady hydrodynamic analysis in animal locomotion. Their valuable analytic solution of the instantaneous inviscid fluid forces acting on the shells of swimming scallops, obtained from thin airfoil theory, described the action of the steady forces and the acceleration reaction. Furthermore, their solution included unsteady terms dependent on shell gape angle and gape angular velocity, which Cheng & DeMont (1996*b*) have called 'pseudoelasticity' and 'pseudoviscosity', respectively. The work was based on high-speed cine records of swimming scallops and has allowed them to describe in detail the kinematics, dynamics and energetics of scallop locomotion. Most importantly, they have produced the first truly *in vivo* muscle force–velocity trajectory, or work loop, in the study of animal locomotion (Cheng & DeMont 1997). The work loop they determined was different from traditionally accepted *in vitro* muscle work loops (Cheng & DeMont 1997).

In this paper, we present an unsteady potential flow analysis of the flow past a swimming squid as part of a larger detailed description of the coordination and dynamic contributions of locomotory structures in squid (Anderson 1998). In addition to the hydrodynamic topics covered in this work, a great deal has been learned about the mechanics of squid locomotion. Mantle deformations and patterns of fin and jet activity were analysed in detail. The intramantle pressures involved in producing the jet and the dynamic requirements of the squid musculature to produce such pressures were calculated from accurate volume flow data (Anderson & DeMont 2000). Jet hydrodynamics were analysed including the unsteady terms of the momentum and Bernoulli equations. In addition, an alternative to Froude efficiency was recommended for the calculation of jet propulsive efficiency in squid. The body kinematics and dynamics, including the hydrodynamic forces determined in this work, were integrated in a comprehensive analysis (Anderson 1998). Waves along the body surface were observed, and are described elsewhere (Anderson 1998).

2. Experimental technique

Long-finned squid, *Loligo pealei*, were recorded swimming in large flumes at the Rinehart Coastal Research Center of the Woods Hole Oceanographic Institution. Specimens of *L. pealei* were caught in Woods Hole Sound and Nantucket Sound using nets or jigs. Lengths of the *L. pealei* caught from shore or boat seldom exceeded 0.40 m. Length, L_s, here means total length from the apex of the mantle to the ends of the arms. Squid diameter at the maximum position ranged from 0.03 to 0.05 m. Squid

of length larger than 0.20 m were chosen to ensure Reynolds numbers high enough ($> 10^4$) to legitimize the assumption that, except for a thin boundary layer, the flow around the squid can be treated as inviscid and irrotational. The pressures calculated in the irrotational region just outside the boundary layer are thereby essentially the same as those acting on the squid surface. Reynolds numbers for the swimming squid were calculated on the basis of total length, L_s.

Data collected from two representative squid are reported in this paper. Morphometrics for the two squid are: (i) squid 1: length 0.356 m, mantle length 0.25 m, wet mass 0.169 kg; (ii) squid 2: length 0.313 m, mantle length 0.222 m, wet mass 0.183 kg. We use the notation squid 1s to stand for squid 1 swimming slowly ($0.25\,m\,s^{-1}$) and squid 1f for squid 1 swimming fast ($0.43\,m\,s^{-1}$). Squid 2f stands for squid 2 swimming fast ($0.38\,m\,s^{-1}$).

Two flumes were used for the swimming experiments: (i) a 20 m oval paddle-wheel flume and (ii) a 17 m linear flume. The paddle-wheel flume has a channel width of 0.50 m, is capable of flow speeds up to about $0.50\,m\,s^{-1}$ and was operated at a depth of 0.15 m. Flow speed measurements in the paddle-wheel flume were obtained by tracking large particles in the seawater or neutrally buoyant objects placed in the flow. The 17 m linear flume has a channel width of 0.60 m, and is capable of flow speeds much higher than *L. pealei* were able to achieve in sustained swimming, i.e. about $0.65\,m\,s^{-1}$. The 17 m flume was operated at a depth of 0.30 to 0.40 m. Laser Doppler anemometry (LDA) was used to determine the flow speed in the flume. Flow speed measurements were made at the approximate depth at which the squid were swimming. In general, squid swam at an average speed equal to the oncoming flume speed. Thus, the squid remained essentially in the same position in the flume. The camera field of view needed only to be 0.05 to 0.10 m longer than the squid, which allowed high resolution of its dimensions and movements. In contrast, filming the same swimming sequences in still water would have required a field of view 1.0 to 1.5 m long. The seawater in the flumes was replaced daily and ranged in temperature from 12 to 15 °C, which is in the range experienced by *L. pealei* in the wild.

The high-speed video records were taken using a Redlake HR500 Motionscope. All swimming sequences acquired were of mantle-leading swimming except for one bout of arms-leading swimming. The camera was operated at 125 or 250 frames per second, storing 512 frames per sequence, allowing video sequences of 4 and 2 s duration, respectively. The video image resolution was 600 pixels × 480 pixels. Sequences where the squid was touching, or even very close to, the flume bottom, walls or free surface were rejected to avoid the effects of wall boundary layers and the free surface. Sequences were also rejected if the animal failed to hold its longitudinal axis perpendicular to the lens. Camera distances were chosen to ensure negligible refractive aberration by the air–wall–water interfaces. Acceptable swimming sequences were downloaded from the camera's RAM to a PC using a National Instruments, IMAQ PCI-1408 frame-grabber working in tandem with LabVIEW and Graftek's IMAQ Vision.

The time-varying outline of the squid profile from each squid swimming sequence was extracted automatically with a PC, frame-by-frame, using a peak grey-level gradient searching algorithm (Anderson 1998). The algorithm subjects images to a standard Prewitt grey-level gradient filter, and then searches the gradient matrix for the contour of maximum gradient that represents the outline of the squid. This works well for high-contrast image sequences. Good contrast was achieved with front lighting and a black felt background.

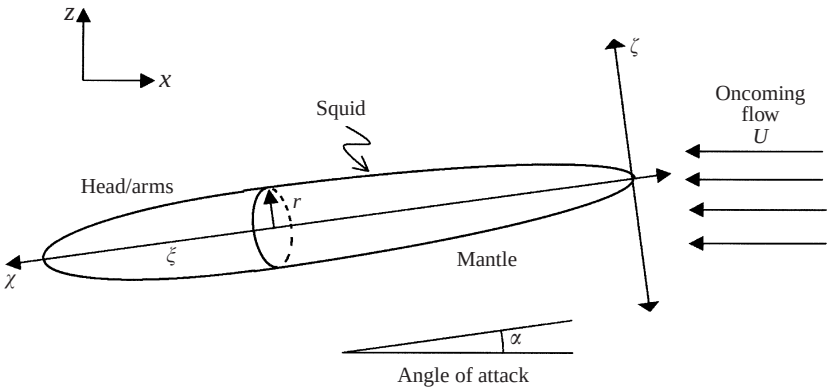

FIGURE 3. Coordinate systems used in the analysis of squid locomotion.

3. Fluid dynamic model

3.1. *Coordinate systems*

Three coordinate systems were used in this analysis (figure 3). The x- and z-axes represent the fixed reference frame of the camera field of view and flume. The flume flow velocity, U, is in the negative x-direction. The squid swam into the flow in the positive x-direction. The z-axis is the vertical position in the water column.

The second coordinate system, the ξ- and ζ-axes, has its origin at the apex of the mantle. Recall that this is the end of the squid which usually leads in sustained swimming and escape responses. The ξ-axis is the long axis of the squid. It extends from $\xi = 0$ at the apex of the mantle to $\xi = L_s$, i.e. squid length, to the tip of the arms. The ξ-direction is referred to as the axial direction; however, the sign of the ξ-direction is used loosely when discussing velocities and accelerations. For example, the term axial velocity is used to describe squid motion in the negative ξ-direction so that axial velocities are reported as positive values. This is simply to prevent confusion in the presentation of velocities and accelerations. The ζ-axis is the transverse axis, or dorso-ventral axis, perpendicular to the ξ-axis and intersecting ξ at the apex of the mantle, i.e. $\xi = 0$.

The third coordinate system (r, θ, χ), which was used for hydrodynamic calculations, is a cylindrical system on account of the axisymmetric treatment of the squid. The long axis of the squid, ξ, lies on the χ-axis and the radius of the squid at any point along the axis is $R = R(\chi, t)$. Note that the ξ and χ positions and directions are the same and therefore interchangeable except that the ξ-axis is limited to the length of the squid, while the χ-axis spans $(-\infty, +\infty)$. In general, squid swam with very small angles of attack so that the x-axis of the first coordinate system was also essentially co-linear with χ. The variable θ is the angle about the χ-axis and does not appear in the squid surface equation, $R = R(\chi, t)$, owing to the axisymmetric shape of the squid. The squid shape as a function of time can be represented by a three-dimensional surface as a function of time and axial position (figure 4).

3.2. *Flow around an axisymmetric body and the small disturbance approximation*

The squid lends itself well to the application of three-dimensional potential flow theory for slender axisymmetric bodies after the method outlined by Karamcheti (1966). The spindle shape of squid, with its pointed ends, reduces the error in the linearization process of the slender body approximation, which assumes small disturbances of the

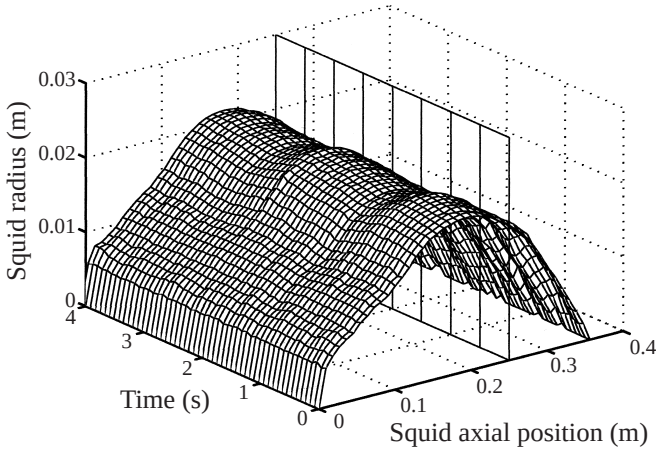

FIGURE 4. Example data set of the surface of a swimming squid (squid 1s) over a 4 s swimming sequence. The squid is treated as axisymmetric and its time-varying surface can therefore be represented by radius as a function of axial position and time, $R = R(\xi, t)$. Note the regular pattern of contraction and expansion of the mantle with time, especially visible at the mid-length position. The 'fence' marks the border between the mantle region and the head and arms region. The longitudinal and radial axes are not drawn to scale.

oncoming flow and small body surface slope with respect to the longitudinal axis. Objects with more rounded edges violate these assumptions. The highly streamlined shape of squid results in a delayed separation point, extending the application of the potential flow solution over a large portion of the body. As in the case of the scallop (Cheng & DeMont 1996*b*), the squid creates a context in the study of animal locomotion for the seldom utilized unsteady terms in the Bernoulli equation and boundary conditions of potential flow theory, giving them practical significance and contributing much to the understanding of the actual dynamics of aquatic locomotion, where steady-state simplifications are often used.

The disturbance potential for a squid swimming at speed $V_s(t)$ in the fixed x, z co-ordinate system of the flume is determined using the body-fixed cylindrical coordinate system (r, θ, χ). The fluid is incompressible, so the continuity equation is

$$\nabla \cdot \boldsymbol{V} = 0. \tag{3.1}$$

Outside the thin boundary layer and wake, the flow field, $\boldsymbol{V}$, is considered irrotational, therefore

$$\nabla \times \boldsymbol{V} = 0. \tag{3.2}$$

The condition of irrotationality allows the velocity field, $\boldsymbol{V}$, to be treated as the gradient of a scalar function,

$$\boldsymbol{V} = \nabla \Phi \tag{3.3}$$

because of the vector identity,

$$\nabla \times \nabla \Phi = 0. \tag{3.4}$$

Substituting (3.3) into the condition of incompressibility (3.1), one obtains the Laplace equation.

$$\nabla^2 \Phi = 0. \tag{3.5}$$

The method of determining velocity fields by potential flow theory involves finding a solution, Φ, to the Laplace equation.

The disturbance potential, ϕ, for a swimming squid was treated as a line distribution of sources and sinks,

$$\phi = -\frac{1}{4\pi}\int_0^{L_s} q(\xi,t)\frac{\mathrm{d}\xi}{\sqrt{(\chi-\xi)^2+r^2}}, \tag{3.6}$$

where $q(\xi,t)$ is the source strength per unit length along the axis of the object being constructed (Karamcheti 1966). This ϕ is a well-known solution of the Laplace equation. From the potential function, ϕ, the radial and axial components of the velocity field caused by the source/sink distribution can be derived,

$$\frac{\partial\phi}{\partial r} = v_r(\chi,r,t) = \frac{1}{4\pi}\int_0^{L_s} q(\xi,t)\frac{r}{[(\chi-\xi)^2+r^2]^{3/2}}\mathrm{d}\xi, \tag{3.7}$$

$$\frac{\partial\phi}{\partial\chi} = v_\chi(\chi,r,t) = \frac{1}{4\pi}\int_0^{L_s} q(\xi,t)\frac{\chi-\xi}{[(\chi-\xi)^2+r^2]^{3/2}}\mathrm{d}\xi, \tag{3.8}$$

where v_r and v_χ are the radial and axial velocities produced by the source/sink distribution. The velocity field, $\boldsymbol{V}(r,\theta,\chi,t)$, and the velocity potential, $\Phi(r,\theta,\chi,t)$, for the flow around the squid shape can then be written as the superposition of the oncoming flow, $\boldsymbol{V}_s(r,\theta,\chi,t)$, and the disturbance, or perturbation, velocity and potential, V_p and ϕ_p respectively,

$$\boldsymbol{V}(r,\theta,\chi,t) = \boldsymbol{V}_s(r,\theta,\chi,t) + \boldsymbol{V}_p(r,\theta,\chi,t), \tag{3.9}$$

$$\Phi(r,\theta,\chi,t) = \phi_s(r,\theta,\chi,t) + \phi_p(r,\theta,\chi,t). \tag{3.10}$$

The oncoming velocity in the squid frame of reference is simply the vector sum of the axial and lateral velocities which were calculated from the trajectory of the squid extracted from the high-speed video records (Anderson 1998). Recall that the sign on the axial velocity is used loosely, therefore it is shown added here rather than subtracted.

We now have the potential function for the flow field around the swimming squid. However, in the above integrals (3.6), (3.7), and (3.8), $q(\xi,t)$ is not known. Boundary conditions must therefore be applied to narrow down the choice of $q(\xi,t)$. The boundary condition used is that of no-penetration. Since there is no flow across the surface of the squid, the normal component of the velocity field must be equal to the normal component of the velocity of the boundary, $\boldsymbol{V}_B$,

$$\nabla\Phi\cdot\boldsymbol{n} = \boldsymbol{V}_B\cdot\boldsymbol{n} \quad \text{on the squid surface.} \tag{3.11}$$

The surface of the squid, treated as axisymmetric, can be represented by

$$F(r,\theta,\xi,t) = r - R(\xi,t) = 0, \tag{3.12}$$

where $R(\xi,t)$, has been derived from the video records and describes the time-varying radius at any position, ξ, on the longitudinal axis (figure 4). Defining the boundary in this way, we obtain a new expression for the no-penetration boundary condition (3.11):

$$\frac{\mathrm{D}F}{\mathrm{D}t} = \frac{\partial F}{\partial t} + \nabla\Phi\cdot\nabla F = 0 \quad \text{on} \quad F(r,\theta,\xi) = 0. \tag{3.13}$$

Resolving $\boldsymbol{V}_s(t)$ into its component vectors and taking account of angle of attack, α, one obtains

$$\boldsymbol{V}_s = \boldsymbol{V}_s(\sin\alpha\sin\theta\,\hat{\boldsymbol{e}}_R + \sin\alpha\cos\theta\,\hat{\boldsymbol{e}}_\theta + \cos\alpha\,\hat{\boldsymbol{e}}_\xi). \tag{3.14}$$

Substituting (3.14) into (3.9) and applying the boundary condition, (3.13), to (3.9) and (3.12) results in

$$-\frac{\partial R}{\partial t} + \boldsymbol{V}_s \sin\alpha \sin\theta + \frac{\partial \phi}{\partial r} - \left(\boldsymbol{V}_s \cos\alpha + \frac{\partial \phi}{\partial \chi}\right)\frac{\partial R}{\partial x} = 0, \tag{3.15}$$

where ϕ is the disturbance potential. Since it is a good approximation to consider the squid to be a slender body and to assume the disturbance field to be very small in comparison to the oncoming flow, it is concluded that $\partial\phi/\partial\chi$ and $\partial R/\partial x$ are relatively small. The product of these two quantities is dropped as a second-order term. This is part I of the slender body approximation. Recognizing that $V\cos\alpha$ and $V\sin\alpha$ are the axial and transverse velocities, respectively, and applying this part I of the slender body approximation, one obtains a linearized expression for the radial component of the disturbance velocity:

$$v_r = \frac{\partial \phi}{\partial r} = \frac{\partial R}{\partial t} - V_\zeta \sin\theta + V_\xi \frac{\partial R}{\partial x}. \tag{3.16}$$

For the very small angles of attack observed in the recorded swimming sequences, x, χ and ξ are co-linear, and the ζ-velocity term contributes only 2 to 3% of the radial disturbance velocity. Ignoring this term results in

$$v_r = \frac{\partial \phi}{\partial r} = \frac{\partial R}{\partial t} + V_\xi \frac{\partial R}{\partial \chi}. \tag{3.17}$$

Knowing the radial disturbance velocity allows one to estimate the value of $q(\xi, t)$ in the integral of (3.7). Consider a small cylinder drawn around a section, $\mathrm{d}\chi$, of the line source distribution. The flow across the sidewall of the cylinder approaches the flow out of the source distribution over that section, $q(\chi, t)\mathrm{d}\chi$, as r becomes small. As r gets smaller, the circular ends of the cylinder get smaller and more of the flow in and out of the distribution goes through the sidewall. Thus, the following connection between v_r and q can be made:

$$2\pi r v_r(\chi, t)\mathrm{d}\chi = q(\chi, t)\mathrm{d}\chi \quad \text{as} \quad r \to 0. \tag{3.18}$$

Taylor series expansion of rv_r at the squid surface about the longitudinal axis verifies the above expression as a reasonable estimate for q for the known slender body (Karamcheti 1966). This is part II of the slender body approximation. One can now substitute q into the earlier integrals, (3.6) and (3.8), to determine the potential, ϕ, and the axial component, v_x, of the disturbance velocity using

$$q(\chi, t) = 2\pi r v_r(\chi, t) = 2\pi R\left(\frac{\partial R}{\partial t} + V_\xi \frac{\partial R}{\partial \chi}\right). \tag{3.19}$$

The integrals were solved piecewise analytically using constant values for R, $\partial R/\partial t$, V_ξ, and $\partial R/\partial\chi$ at approximately 400 axisymmetric ring panels on the squid surface for each of the 512 frames of the video sequence. The result is the velocity field near the surface of the squid for the entire swimming sequence. Part II of the slender body approximation restricts the knowledge of the velocity field to the surface of the squid, but this contains the important hydrodynamic information. With it, the time-varying pressures acting over the entire squid surface, and the resulting hydrodynamic forces, were calculated.

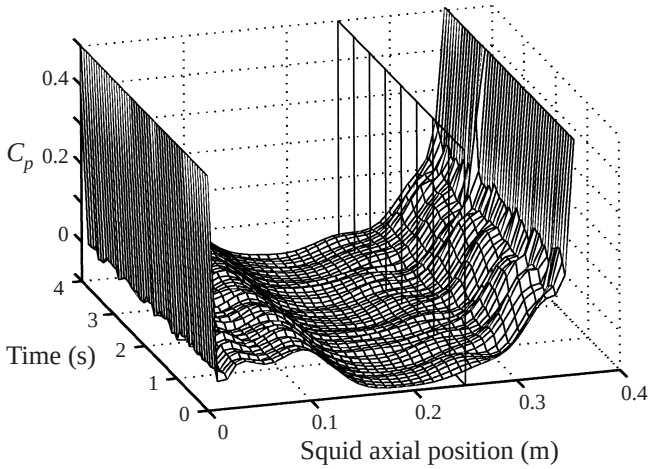

FIGURE 5. Pressure coefficient, C_p, over the surface of squid 1s for an entire swimming sequence. The 'fence' marks the border between the mantle region and the head and arms region. The coefficient is equal to 1 at the leading and trailing ends of the squid.

4. Hydrodynamic loads

Surface pressure coefficients were determined using the unsteady form of the Bernoulli equation, rearranged to yield

$$C_p(\xi,t) \equiv \frac{p-p_\infty}{\frac{1}{2}\rho V_\infty^2} = 1 - \frac{1}{V_\infty^2}\left([V(\xi,t)]^2 + 2\frac{\partial\phi(\xi,t)}{\partial t}\right), \tag{4.1}$$

where V_∞ is the axial velocity of the squid (i.e. V_ξ), and $V(\xi,t)$ is the magnitude of the velocity of the fluid at the squid surface, with respect to the squid. Equation (4.1) results in pressure coefficients over the entire length of the squid for the entire swimming sequence. Figure 5 shows the pressure coefficients, C_p, over the surface of squid 1s, during the entire swimming sequence ($U = 0.25\,\mathrm{m\,s^{-1}}$). These pressure coefficients are in reasonable agreement with steady experimental measurements made on an axisymmetric squid model by Vogel (1987). Cross-sections of the pressure coefficient plot (figure 6) suggest that instantaneous body shape, i.e. the quasi-steady effect, has a greater impact on C_p than changes in body shape over time. In general, lower pressure coefficients occur when and where body surface curvature is most convex, as is expected in a steady case. Nevertheless, there are instances where this is not strictly the case (figure 6*b*, *c* at $t = 3.4\,\mathrm{s}$).

The pressure coefficients were used to calculate excess pressure on the surface of the squid, p_s, using

$$p_s(\xi,t) = \tfrac{1}{2}C_p(\xi,t)\rho[V_\xi(t)]^2. \tag{4.2}$$

Figure 7(*a*) shows an example of the surface pressures on squid 1s, at the beginning and end of a jet event. The pressures can be used to examine flow-assisted refilling (Vogel 1987). Volume flow rate measurements (Anderson & DeMont 2000) and estimates of intake orifice size can be used to make rough estimates of refill pressures using the Bernoulli equation. At the swimming speeds reported here (0.25–0.43 $\mathrm{m\,s^{-1}}$), these estimates range from -10 to $-100\,\mathrm{Pa}$. From figure 7(*a*), the assistance of the negative pressures ($\sim -4\,\mathrm{Pa}$) around the mantle would be 4–40% at $U = 0.25\,\mathrm{m\,s^{-1}}$. However, the pressure at the mantle intake aperture is about $-2\,\mathrm{Pa}$. Therefore the flow assistance to mantle refilling is reduced to 2–20%. At $U = 0.38\,\mathrm{m\,s^{-1}}$ (figure 7*b*),

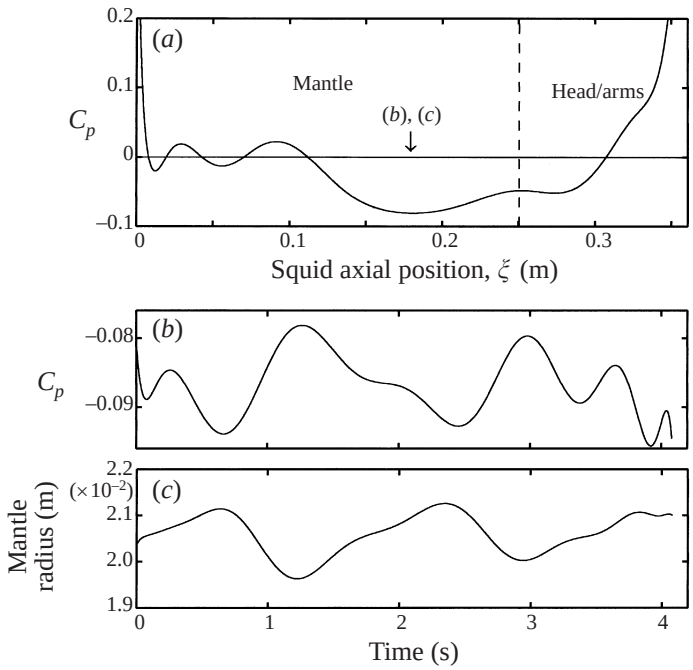

FIGURE 6. (*a*) Pressure coefficient, C_p, along squid 1s, for a particular instant, $t = 1.2$ s, during the swimming sequence. The dashed line marks the border between the mantle region and the head and arms region. (*b*) Pressure coefficient vs. time on the surface of squid 1s at the middle of the squid, $\xi = 0.18$ m, over the entire swimming sequence. (*c*) Squid radius vs. time at the same position from squid 1s.

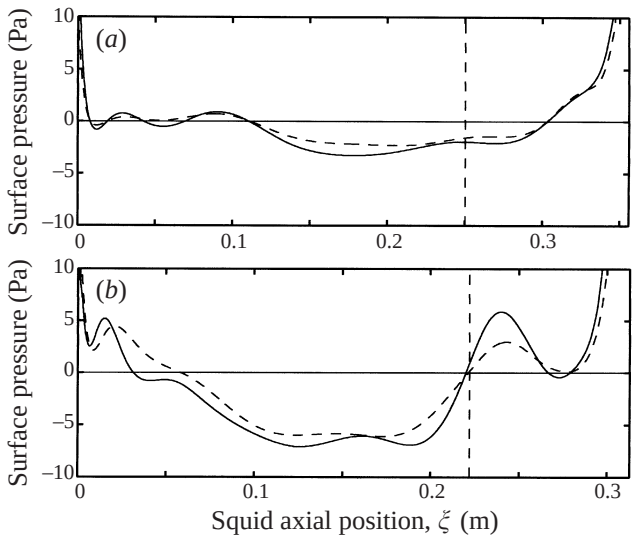

FIGURE 7. Surface pressure along (*a*) squid 1s and (*b*) squid 2f at two different moments during the swimming sequence. The dashed line represents the pressures at the onset of a jet period when the squid is completing its refill period and moving slowly. The solid line shows the pressures at the end of a jet cycle when the squid is moving more quickly. Note that the pressures are slightly greater in magnitude at the end of the jet period – when the squid is moving faster.

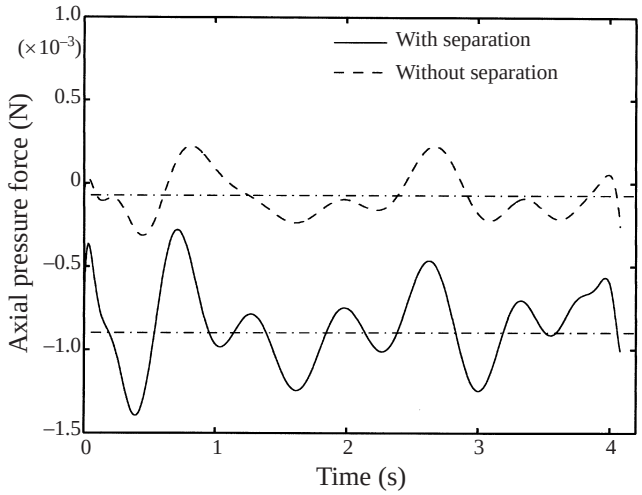

FIGURE 8. The axial pressure force with and without separation acting on squid 1s over the entire swimming sequence. Negative axial force acts in the opposite direction to the axial velocity of the squid. Dash-dotted lines represent the full locomotory cycle averages for the two forces. The average axial pressure force without separation is close to zero as woud be expected in ideal steady flow.

negative pressures around the mantle (~ -5 Pa) together with a positive intake aperture pressure (~ 5 Pa) results in a potential for assistance in mantle refill of about 10 Pa, or 10–100%. However, the positive pressure at the intake aperture may be an artifact of the axisymmetric rendering of the squid beyond the mantle. A rapid decrease in average radius just aft of the mantle was observed in some swimming sequences owing to the asymmetry between the dorsal and ventral body surfaces. This would result in a steeply increasing calculated pressure coefficient at this position. In reality, there is a fairly smooth transition of the dorsal body surface from the mantle to the head, and a more step-like transition on the ventral surface. Rather than a positive pressure, one would expect separation as in a downward step and a low pressure in the recirulating region behind the step. Therefore, it is safe to assume that the assistance in mantle refill is closer to 5 Pa, or 5–50% of the refill pressure.

4.1. *Axial pressure force*

Flow-induced surface pressures were used to determine the total axial pressure force, F_p, acting on swimming squid using

$$F_p(t) = \frac{\pi}{4}\int_0^S p_s(\xi,t)D(\xi,t)\frac{\partial D(\xi,t)}{\partial \xi}\mathrm{d}\xi - \frac{\pi}{4}p_s(S,t)[D(S,t)]^2, \tag{4.3}$$

where $\xi = S$ is the separation point approximated from our digital particle image velocimetry (DPIV) data of squid swimming. The time-varying axial fluid force both with and without separation is shown for squid 1s in figure 8. The forces are shown as negative values since they are directed against the motion of the squid. The force with separation ranges from 0.0003 to 0.0014 N, with an average of 0.0009 N.

As expected, the average pressure force assuming no separation is essentially zero and reveals that the majority of the small axial pressure force is form drag or pressure drag. In a quasi-steady analysis without separation the axial fluid force would be zero and constant. The fluctuations in this value in figure 8 are the result of the unsteady analysis performed. In the unsteady analysis, the acceleration of the squid and the rate

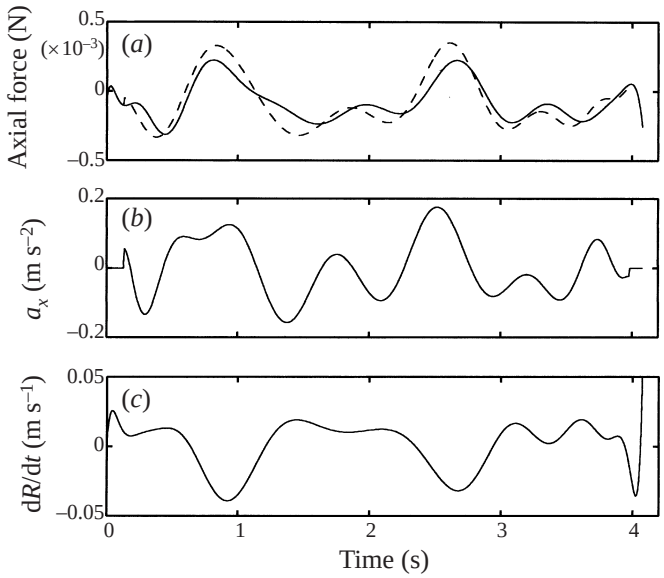

FIGURE 9. Plots of (*a*) axial pressure force without separation, (*b*) axial acceleration and (*c*) rate of deformation at $\xi = 0.18$ m. The dashed line in (*a*) represents the axial pressure force when an estimate for added mass ($\alpha_m = 0.01$) is chosen and the acceleration reaction subtracted. The resulting force curve resembles the opposite of the rate of deformation and suggests its importance in the determination of the unsteady part of the axial pressure force.

of deformation of the squid impact the surface pressures calculated. A comparison of the axial pressure force without separation to squid acceleration and rate of deformation at mid-body suggests that rate of deformation is the more significant factor (figure 9). The so-called acceleration reaction appears to play a negligible role at the swimming speeds observed. The acceleration reaction can be written as

$$F_{AR} = -\alpha_m m a, \tag{4.4}$$

where α_m is the added mass coefficient, m is the mass of the fluid displaced by the body and a is the acceleration of the body through the fluid. The force acts in the opposite direction to the acceleration of the body. This means that the contribution of the acceleration reaction is positive when a body is decelerating. If the acceleration reaction were significant, one would expect the axial fluid force without separation to be the opposite of the acceleration curve. Instead, the axial pressure force is more similar to the opposite of the rate of change of the mantle radius. This similarity can be explained by the unsteady term in equation (4.1), since ϕ in our numerical solution is proportional to $-R(x, t)$. This results in a higher pressure when and where the body is expanding and therefore a higher pressure drag since the leading end of the squid, the mantle, is the expanding region. When the mantle contracts the result is a low pressure that actually contributes minutely to thrust. If an added mass coefficient on the order of 0.01 is assumed and the acceleration reaction predicted using that value is subtracted, the remaining axial fluid force closely matches the opposite of the shape of the rate-of-deformation curve (figure 9). For any body, the acceleration reaction is dependent on shape. It is greatest in bluff bodies. The apparent insignificance of the acceleration reaction in squid locomotion can be attributed to the streamlined shape of squid.

Remarkably, the axial pressure force calculated here is only about 3% of the minimum drag force determined from the net axial force on the swimming squid, i.e. $F = ma$ (Anderson 1998), and suggests that flow-induced pressures on the squid body surface as a whole play a negligibly small role in resisting squid motion. This means that the dominant sources of drag in squid locomotion are friction drag on the body and fins, and the force due to the intake of fluid into the mantle. It is likely that pressure forces due to the motion of the fins sometimes act against the forward motion of the squid, as well, should the fins be used for braking, turning (Williamson 1965), or should the squid use its forward motion through the fluid to passively re-cock its fins for a subsequent downstroke (Anderson 1998). The inviscid analysis performed here does not include friction drag or the fin, jet and refill forces; it is simply concerned with the effect of body shape and body kinematics. Figure 10 shows the net axial force acting on squid 1s compared to the calculated axial pressure force, and quasi-steady skin friction estimated for laminar and turbulent boundary layers over the axisymmetric squid including the fins. Since the net force during refill is consistently more negative than either laminar or turbulent skin friction, mantle refill must involve a significant force resisting the motion of swimming squid. A complete viscous analysis would be necessary to determine the skin friction accurately. We have used flat-plate friction for both turbulent and laminar flow as a rough approximation here. Over the body of the slender squid, pressure gradients are small, and this should be a good approximation. The use of flat-plate friction on the undulating fins is tenuous, but even doubling the friction contributed by the fins – as might be suggested by recent boundary layer measurements over undulating fish (Anderson, McGillis & Grosenbaugh 2001) – would not fully account for the negative forces observed during mantle refill, especially if the flow is laminar (figure 10). Therefore we expect the same conclusions concerning the significance of skin friction and mantle refill even if a more accurate determination of skin friction were performed.

The small form drag observed is explained simply by the very streamlined shape of the squid. Separation is very far to the rear, but even taking the separation point at more forward positions than those used here leads to small drag values. Overall, form drag depends on the amount by which an object disturbs the oncoming flow. Since the velocity is disturbed very slightly by the slender squid, the pressure differences which contribute to form drag are themselves quite small. It should be mentioned that although a constant separation point has been selected here, its real location very likely oscillates. The changing velocities of the flow over the mantle and mantle intake most certainly cause some shifting of the separation point. Mantle intake may act as boundary layer suction, as suggested by Zuev (1964). The suction of 'tired' particles out of the boundary layer may serve to thin the boundary layer and decrease the susceptibility of the flow to separation.

4.2. *Lateral fluid forces*

From the flow-induced surface pressures, lateral forces acting on the squid mantle were calculated. The lateral force due to surface pressures is

$$F_{LAT} = p_s A_{LAT} = p_s LD, \tag{4.5}$$

where A_{LAT} is the laterally projected area of a mantle ring with length, L, and outer diameter, D. The necessary circumferential muscle force in the mantle wall is then decreased by the amount

$$F_{cFluid} = \tfrac{1}{2} p_s DL \tag{4.6}$$

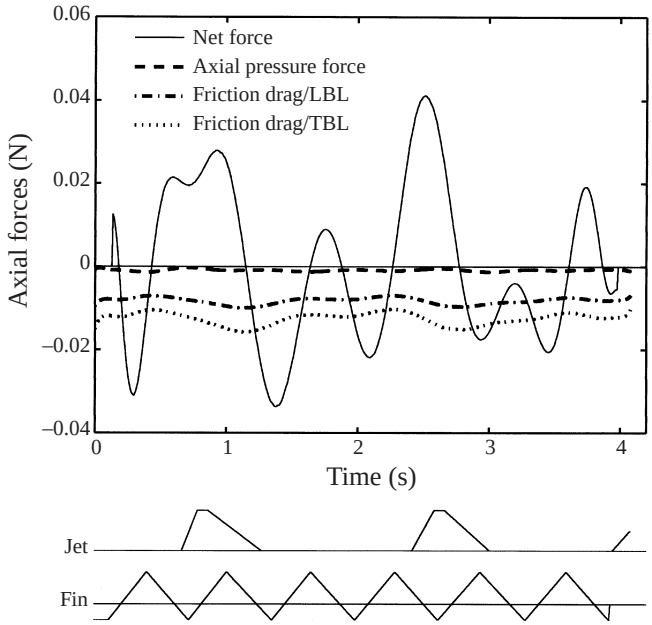

FIGURE 10. Comparison of instantaneous axial pressure force, estimated skin friction (body and fin surfaces) for both a laminar (LBL) and a turbulent boundary layer (TBL) treatment, and net force. Jet and fin activity are included. Periods between jet pulses are when refill occurs. On the fin activity plot an upward slope represents an upstroke while a downward slope represents a downstroke. Note that negative forces cannot be explained by pressure or friction drag alone. Large negative forces occur during refill (e.g. $t = 0.3$, 1.4 and 2.1 s). Fin downstrokes in the middle of the refill periods work against these negative forces, even resulting in a short period of positive net force in the first complete refill period ($t = 1.6$–1.9 s). This points out the significant role of the fins at this swimming speed ($U = 0.25\,\mathrm{m\,s^{-1}}$).

for the ring in question owing to the fluid flow. Hence, positive excess pressures reduce the circular muscle forces necessary to contract and negative excess pressures increase the load on the circular muscles. The convex shape of the mantle over its anterior region results in negative excess pressures and therefore the flow-induced surface pressures work against the circular muscles in contraction, and work with the recoil mechanism during refill, as described by Vogel (1987). The contribution of lateral fluid forces to the circumferential mantle forces can be expressed for a particular region $[\xi_1, \xi_2]$ using the following integral:

$$F_{cFluid}(t) = \tfrac{1}{2} p_s(\xi, t) \int_{\xi_1}^{\xi_2} D(\xi, t)\,\mathrm{d}\xi. \tag{4.7}$$

The time-varying lateral force per centimetre of body length due to radial fluid forces acting at $\xi = 0.75\ L_m$ is shown for squid 1s in figure 11. The behaviour of the force is opposite to that of the axial velocity (figure 11). This can be understood from the perspective of the steady Bernoulli equation. The higher-velocity flow over the convex surface of the squid leads to lower pressure and therefore a more negative force.

The effect of these lateral forces was included in the determination of the *in vivo* muscle work loop presented elsewhere (Anderson 1998). The negative forces tend to pull the mantle open and increase the minimum required muscle tensions over any jet cycle. However, since the intramantle mantle fluid pressures were found to be on the order of 10^2 to 10^3 (Anderson & DeMont 2000), and flow-induced surface pressures

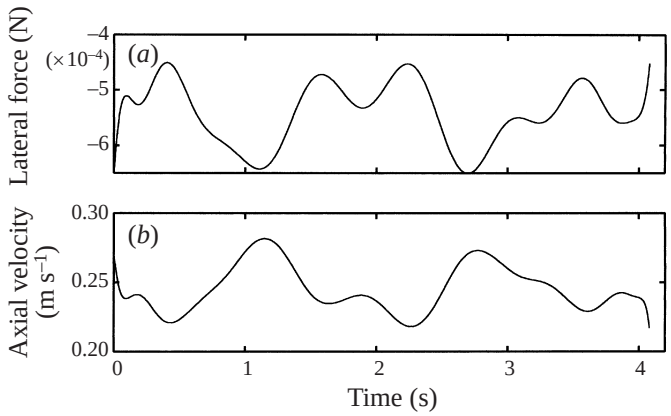

FIGURE 11. (*a*) Lateral pressure force per 0.01 m on the mantle of squid 1s at $\xi = 0.75\,L_m$ for the entire swimming sequence. This force is negative due to the negative pressures on the mantle surface. The circular muscles have to exert extra force to overcome this force during contraction. During refill, this force would tend to draw the mantle open, but as stated when discussing refill pressures, the contribution of this hydrodynamic force in refill is probably less than 1%. Lateral pressure forces resemble the opposite of the axial velocity (*b*) as would be expected under the steady Bernoulli equation.

in this work are on the order of 10°, the impact of exterior fluid forces on the work loop was minimal, on average $< 1\%$.

5. Conclusion

The squid body shape results in remarkably small form drag and added mass effects according to the potential flow analysis described here. The effects are so small that even a choice of the separation point at the position of maximum diameter results in essentially negligible drag. Analyses of hydrodynamic drag on swimming squid should therefore concentrate on accurate determinations of skin friction and negative forces due to the mantle refill period (Anderson 1998). There is evidence from a hydrodynamic analysis of squid jetting that unsteady effects involved in the jet event may also lead to negative forces (Anderson & DeMont 2000).

The importance of friction drag raises questions about possible friction drag reducing methods. The observation of body surface waves along the mantle of squid (Anderson 1998) introduces the interesting possibility that the squid is manipulating the boundary layer flow for increased hydrodynamic efficiency. Studies of flow over waving plates show that separation can be suppressed and boundary layers laminarized by such body surface movements (Taneda & Tomonari 1974; Anderson *et al.* 2001). The skin friction would be significantly lower for a laminar boundary layer over the squid resulting in large savings over long migrations (Anderson 1998). Perhaps the squid also benefits from the boundary layer stabilizing properties observed for compliant surfaces (Carpenter 1998) and suggested for dolphins (Kramer 1960).

The relatively simple system of the squid has made the present unsteady hydrodynamic analysis of aquatic animal locomotion possible without computational fluid dynamics. The approach simply requires accurate swimming data and basic numerical techniques. This was intentional so as to develop a widely accessible tool for the investigators of squid locomotion. Fully viscous computational studies, for example Carling, Williams & Bowtell (1998), would be useful to determine the magnitude of

the negative forces due to refill observed in this work accurately, since such analyses result in more accurate determinations of axial pressures forces and viscous drag.

This project was funded by a Natural Sciences and Engineering Research Council of Canada grant to M. E. D., who also received support from the Ester A. and Joseph Klingenstein fund from the Marine Biological Laboratory (MBL, Woods Hole), and a W. J. Fulbright Scholarship to E. J. A. We thank R. K. O'Dor at Dalhousie University; J. P. Quinn, E. C. Oguejiofor, and P. MacGillivray at St. Francis Xavier University; T. L. Daniel at the University of Washington; S. Gallagher, M. Grossenbaugh, W. McGillis and the staff at the Rhinehart Coastal Research Center of the Woods Hole Oceanographic Institution, and R. Hanlon at MBL for technical assistance and advice.

REFERENCES

Aleev, Y. G. 1962 Position of the greatest height in the body of fish. *Zool. J.* **41**, 1429–1431.

Anderson, E. J. 1998 The mechanics of squid locomotion. MSc thesis, St. Francis Xavier University, Nova Scotia, Canada.

Anderson, E. J. & DeMont, M. E. 2000 The mechanics of locomotion in the squid *Loligo pealei*. Locomotory function and unsteady hydrodynamics of the jet and intramantle pressure. *J. Expl Biol.* **203**, 2851–2863.

Anderson, E. J., McGillis, W. R. & Grosenbaugh, M. A. 2001 The boundary layer of swimming fish. *J. Expl Biol.* **204**, 81–102.

Bradbury, H. E. & Aldrich, F. A. 1969 Observations on locomotion on the short-finned squid, *Illex illecebrosus illecebrosus* (Lesueur, 1821), in captivity. *Can J. Zool.* **47**, 741–744.

Carling, J., Williams, T. L. & Bowtell, G. 1998 Self-propelled anguilliform swimming: simultaneous solution of the two-dimensional Navier-Stokes equations and Newton's laws of motion. *J. Expl Biol.* **201**, 3143–3166.

Carpenter, P. W. 1998 Current status of the use of wall compliance for laminar-flow control. *Expl Therm. Fluid Sci.* **16**, 133–140.

Cheng, J.-Y., Davison, I. G. & DeMont, M. E. 1996 Dynamics and energetics of scallop locomotion. *J. Expl Biol.* **199**, 1931–1946.

Cheng, J.-Y. & DeMont, M. E. 1996*a* Jet-propelled swimming in scallops: swimming mechanics and ontogenic scaling. *Can. J. Zool.* **74**, 1734-1748.

Cheng, J.-Y. & DeMont, M. E. 1996*b* Hydrodynamics of scallop locomotion: unsteady fluid forces on clapping shells. *J. Fluid Mech.* **317**, 73–90.

Cheng, J.-Y. & DeMont, M. E. 1997 A predicted *in vivo* muscle force-velocity trajectory. *Can J. Zool.* **75**, 371–375.

Cole, K. S. & Gilbert, D. L. 1970 Jet propulsion of squid. *Biol. Bull.* **138**, 245–246.

Daniel, T. L. 1984 Unsteady aspects of aquatic locomotion. *Am. Zool.* **24**, 121–134.

Gosline, J. M. & DeMont, M. E. 1985 Jet-propelled swimming in squid. *Sci. Am.* **252**, 96–103.

Gosline, J. M. & Shadwick, R. E. 1983 The role of elastic energy storage mechanisms in swimming: an analysis of mantle elasticity in escape jetting in the squid, *Loligo opalescens*. *Can J. Zool.* **61**, 1421–1431.

Gosline, J. M., Steeves, J. D., Harman, A. D. & DeMont, M. E. 1983 Patterns of circular and radial mantle muscle activity in respiration and jetting of the squid. *J. Expl Biol.* **104**, 97–109.

Hoar, J. A., Sim, E., Webber, D. M. & O'Dor, R. K. 1994 The role of fins in the competition between squid and fish. In *Mechanics and Physiology of Animal Swimming* (ed. L. Maddock, Q. Bone & J. M. V. Rayner), pp. 27–43. Cambridge University Press.

Johnson, W. & Soden, P. D. 1966 The discharge characteristics of confined rubber cylinders. *Intl J. Mech. Sci.* **8**, 213–225.

Johnson, W., Soden, P. D. & Trueman, E. R. 1972 A study in jet propulsion: an analysis of the motion of the squid, *Loligo vulgaris*. *J. Expl Biol.* **56**, 155–165.

Karamcheti, K. 1966 *Principles of Ideal-Fluid Aerodynamics*. John Wiley & Sons.

Kramer, M. O. 1960 Boundary layer stabilization by distributed damping. *J. Am. Soc. Nav. Engrs* **72**, 25–33.

Lane, F. W. 1957 *Kingdom of the Octopus*. Jarrods.

Lighthill, M. J. 1960 Note on the swimming of slender fish. *J. Fluid Mech.* **9**, 305–317.

O'Dor, R. K. 1982 Respiratory metabolism and swimming performance of the squid, *Loligo opalescens*. *Can. J. Fish. Aqua. Sci.* **39**, 580–587.

O'Dor, R. K. 1988 The forces acting on swimming squid. *J. Expl Biol.* **137**, 421–442.

Packard, A. 1969 Jet propulsion and the giant fibre response of *Loligo*. *Nature*. **221**, 875–877.

Packard, A. & Trueman, E. R. 1974 Muscular activity of the mantle of *Sepia* and *Loligo* (Cephalopoda) during respiratory movements and jetting, and its physiological interpretation. *J. Expl Biol*. **61**, 411–419.

Shevtsov, G. A. 1973 Results of tagging of the Pacific squid *Todarodes pacificus* Steenstrup in the Kuril Hokkaido region. *Izv. Tikhookean. Nauchno-Issled Inst. Rybn. Khoz. Okeanogr.* **87**, 120–126 (English transl. *Can. Fish. Mar. Serv. Transl. Ser.* 3300 (1974).)

Siekmann, J. 1962 On a pulsating jet from the end of a tube, with application to the propulsion of certain aquatic animals. *J. Fluid Mech.* **151**, 399–418.

Taneda, S. & Tomonari, Y. 1974 An experiment on the flow around a waving plate. *J. Phys. Soc. Japan* **36**, 1683–1689.

Trueman, E. R. & Packard, A. 1968 Motor performances of some cephalopods. *J. Expl Biol.* **49**, 495–507.

Vogel, S. 1987 Flow-assisted mantle cavity refilling in jetting squid. *Biol. Bull.* **172**, 61–68.

Ward, D. V. 1972 Locomotory function of the squid mantle. *J. Zool. Lond.* **167**, 487–499.

Ward, D. V. & Wainwright, S. A. 1972 Locomotory aspects of squid mantle structure. *J. Zool. Lond.* **167**, 437–449.

Weihs, D. 1973 Mechanically efficient swimming techniques for fish with negative buoyancy. *J. Mar. Res.* **31**, 194–209.

Weihs, D. 1977 Periodic jet propulsion of aquatic creatures. *Fortschr. Zool.* **24**, 171–175.

Williamson, G. R. 1965 Underwater observations of the squid *Illex illecebrosus* Lesueur in Newfoundland waters. *Can. Field Natur.* **79**, 239–247.

Wilson, D. M. 1960 Nervous control of movement in cephalopods. *J. Expl Biol.* **37**, 57–72.

Zuev, G. V. 1963 On the specific gravity of the squid *Ommastrephes sagittatus* Lamarck. *Trudy Sevastopol' skoi Biologicheskoi Stantsii.* **16**. (English transl. Foreign Languages Division, Department of the Secretary of State of Canada.)

Zuev, G. V. 1964 The body shape of cephalopoda. *Trudy Sevastopolsko. Biologicheskoi Stansii.* **17**, 379–387. (English transl. G. A. Thompson.)

Zuev, G. V. 1965 Concerning the mechanism involved in the creation of a lifting force by the bodies of cephalopod molluscs. *Biofizika, Akademiya Nayk SSSR*. **10**, 360–361. (English transl. Foreign Languages Division, Department of the Secretary of State of Canada.)

Zuev, G. V. 1966*a* Turbulent character of the flow around the squid *Ommastrephes sagittatus* Lam. *Biologicheskie Nauki.* **1**, 14–17. (English transl. Foreign Languages Division, Department of the Secretary of State of Canada.)

Zuev, G. V. 1966*b* Characteristic features of the structure of cephalopod molluscs associated with controlled movements. *Ekologo-morfologicheskie issledovaniya nektonnykh zhivotnykh.* Special publication. (English transl. Foreign Languages Division, Department of the Secretary of State of Canada.)